Intermittent stickiness synchronization

Rafael M. da Silva,[1,*] Cesar Manchein,[2,†] and Marcus W. Beims[1,3,‡]
[1]*Departamento de Física, Universidade Federal do Paraná, 81531-980 Curitiba, Paraná, Brazil*
[2]*Departamento de Física, Universidade do Estado de Santa Catarina, 89219-710 Joinville, Santa Catarina, Brazil*
[3]*Max-Planck Institut für Physik Komplexer Systeme, Nöthnitzer Straße 38, 01187 Dresden, Germany*

(Received 29 November 2018; revised manuscript received 25 April 2019; published 13 May 2019)

This work uses the statistical properties of finite-time Lyapunov exponents (FTLEs) to investigate the intermittent stickiness synchronization (ISS) observed in the mixed phase space of high-dimensional Hamiltonian systems. Full stickiness synchronization (SS) occurs when all FTLEs from a chaotic trajectory tend to zero for arbitrarily long time windows. This behavior is a consequence of the sticky motion close to regular structures which live in the high-dimensional phase space and affects all unstable directions proportionally by the same amount, generating a kind of collective motion. Partial SS occurs when at least one FTLE approaches zero. Thus, distinct degrees of partial SS may occur, depending on the values of nonlinearity and coupling parameters, on the dimension of the phase space, and on the number of positive FTLEs. Through filtering procedures used to precisely characterize the sticky motion, we are able to compute the algebraic decay exponents of the ISS and to obtain remarkable evidence about the existence of a universal behavior related to the decay of time correlations encoded in such exponents. In addition we show that even though the probability of finding full SS is small compared to partial SSs, the full SS may appear for very long times due to the slow algebraic decay of time correlations in mixed phase space. In this sense, observations of very late intermittence between chaotic motion and full SS become rare events.

DOI: 10.1103/PhysRevE.99.052208

I. INTRODUCTION

Synchronization in high-dimensional Hamiltonian systems has been defined as a measure synchronization in Refs. [1,2]. In these works the authors use models consisting of two coupled maps. By starting two distinct initial conditions from the uncoupled system, which lead to a regular dynamics, they observe what happens to them by adding a small coupling between the maps. A kind of synchronized (collective) motion appears named *measure synchronization*. As with the synchronization of dissipative chaotic systems [3,4], synchronization in generic Hamiltonian systems is also an interesting issue since such systems present a mixed phase-space dynamics which contains a rich variety of behaviors. However, it is important to mention that the synchronization phenomenon observed in dissipative systems is not possible in Hamiltonian systems due to the Liouville theorem that prevents the full collapse of the orbits to an invariant manifold, since volume must be preserved in phase space.

For symplectic two-dimensional maps the chaotic component is clearly separated from the regular motion [5,6]. However in higher dimensions the chaotic trajectory may visit ergodically the whole phase space but, until this happens, it may suffer a dynamical trapping (or sticky motion) [7,8] close to quasiregular structures. The effect of the sticky motion on the chaotic trajectory can be classified in distinct *regimes* [9,10], defined by the spectrum of finite-time local Lyapunov exponents (FTLLEs). When all FTLLEs are positive, the regime is chaotic; when all are zero, we have an ordered regime. In between we have semiordered regimes. Separating the dynamics in distinct regimes, like a filtering procedure, not only a substantial increase in the characterization of the sticky motion was achieved [11], but this also allowed finding a synchronized-like state, leading to the *intermittent stickiness synchronization* (ISS) discussed in the present work. Essentially the ISS is characterized by the intermittent behavior between the chaotic motion and a kind of transient measure synchronization generated by stickiness. Such synchronized-like states due to stickiness were also detected some years ago and classified as *common motion* [12]. A somewhat similar analysis allowed one to synchronize drive and slave coupled standard maps [13]. In this case, since the coupling between the two maps is unidirectional, once the synchronized state is reached, it does not change along the simulations. Such behavior changes when the coupling interaction between the maps is bidirectional, as considered in the present work, which uses global (all-to-all) interactions.

Since events with long times are associated with times for which the trajectory was trapped to the nonhyperbolic components of the phase space [8,14–18], in the present work the ISS decay is qualitatively described using the time decay of the ordered regime in the case of coupled maps. We mention that other alternative approaches using finite-time Lyapunov exponents (FTLEs) [19–25] can be used to characterize the phase space of conservative systems, with recent applications using large deviation techniques [26–28] and the cumulants [12,29] of the FTLEs distribution.

Recently, a methodology that uses time series of local Lyapunov exponents to define the above mentioned regimes

*rmarques@fisica.ufpr.br
†cesar.manchein@udesc.br
‡mbeims@fisica.ufpr.br

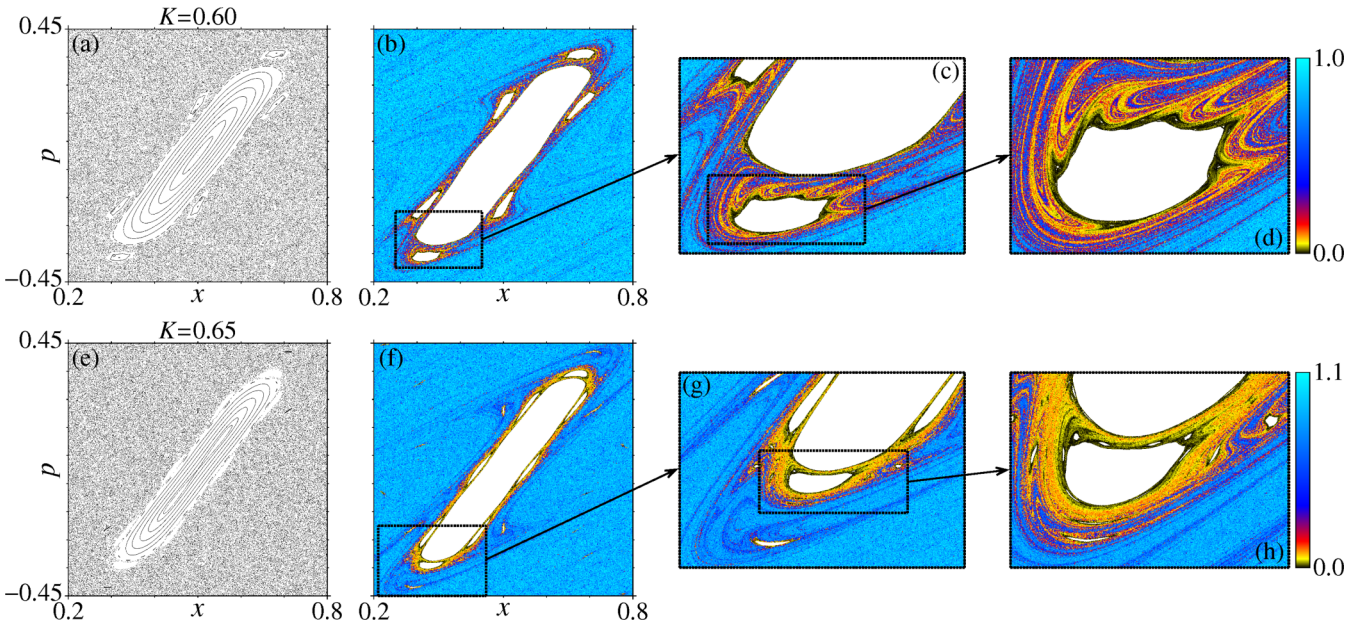

FIG. 1. Phase-space dynamics for the uncoupled case ($\xi = 0$) using (a)–(d) $K = 0.60$ and (e)–(h) $K = 0.65$. In panels (a) and (e) we used 60 initial conditions, each one iterated 8×10^5 times. In (b) and (f) the colors (see the color bar) represent $\lambda_1^{(\omega)}$, for $\omega = 100$, computed through a trajectory of 4×10^8 iterations. Panels (c), (d) and (g), (h) are magnifications of the cases $K = 0.60$ and $K = 0.65$, respectively.

of ordered, semiordered, and totally chaotic motion was proposed, making it possible to improve the characterization of stickiness in Hamiltonian systems with few degrees of freedom [11] and in non-Hamiltonian [30] systems.

The present work uses such filtering procedure [11] to check precisely the algebraic decay exponents of the ISS in higher-dimensional Hamiltonian systems. This investigation is motivated by the low number of numerical studies related to weakly chaotic properties and consequently the long time correlations observed in higher-dimensional mixed phase spaces of Hamiltonian systems (at least for small and moderate numbers of homogeneously coupled two-dimensional maps). We find that only the full stickiness synchronization (SS) obeys a power-law decay, while all other partial SSs decay exponentially. Thus, sticky effects from the semiordered regimes are almost irrelevant for long time ISS decay. Additionally, the algebraic decay exponent of full SS seems to be independent of (i) the number of coupled maps (at least for a moderate number of them), and (ii) the coupling intensities used here. Although it is still under debate whether such an exponent persists in the weak-coupling regime, our investigation corroborates the claim suggested in [27] that predicts the existence of a *generic* decay exponent for time correlations $\chi \sim 0.20$ for Hamiltonian systems with few degrees of freedom, which is smaller than what is given in the conjecture proposed in [16] to predict the existence of a universal decay of Poincaré recurrences with $\gamma \approx 1.30$–1.40 (see also [31] for earlier work). The corresponding relationship between these algebraic exponents is given by the well-known equation $\chi = \gamma - 1$.

The plan of this paper is presented as follows. Section II presents the coupled-map model used for the simulations. In Sec. III the precise definition of ordered, semiordered, and chaotic regimes is given, which leads to the definition of the synchronized-like state, together with some numerical examples. In Sec. IV the ISS decay is discussed qualitatively, and Sec. V summarizes our conclusions.

II. COUPLED-MAP MODEL

Consider the time-discrete composition $\mathbf{T} \circ \mathbf{M}$ of the independent one-step iteration of N symplectic 2-dimensional maps $\mathbf{M} = (M_1, \ldots, M_N)$ and a symplectic coupling $\mathbf{T} = (T_1, \ldots, T_N)$. This constitutes a $2N$-dimensional Hamiltonian system. For our numerical investigation we use the 2-dimensional standard map (SM)

$$\mathbf{M_i}\begin{pmatrix} p_i \\ x_i \end{pmatrix} = \begin{pmatrix} p_i + K_i \sin(2\pi x_i) & \mod 1 \\ x_i + p_i + K_i \sin(2\pi x_i) & \mod 1 \end{pmatrix}, \quad (1)$$

and for the coupling,

$$\mathbf{T_i}\begin{pmatrix} p_i \\ x_i \end{pmatrix} = \begin{pmatrix} p_i + \sum_{j=1}^{N} \xi_{i,j} \sin[2\pi(x_i - x_j)] \\ x_i \end{pmatrix}, \quad (2)$$

with $\xi_{i,j} = \xi_{j,i} = \frac{\xi}{\sqrt{N-1}}$ (all-to-all coupling). This system is a typical Hamiltonian benchmark tool with mixed phase space presenting all essential features expected in complex systems. It was studied in Refs. [15,32] using the recurrence time statistic (RTS) and used in Ref. [11] to propose the classification of Lyapunov regimes for improving stickiness characterization. In all numerical simulations we used nonlinearity parameters corresponding to a mixed phase space, namely $0.60 \leqslant K \leqslant 0.65$ (see Fig. 1, which is discussed next).

III. DEFINITION OF REGIMES AND STICKINESS SYNCHRONIZATION

The numerical technique uses the FTLLEs spectrum $\{\lambda_{i=1\ldots N}^{(\omega)}\}$ computed along a chaotic trajectory during a

window of size ω, where $\lambda_1^{(\omega)} > \lambda_2^{(\omega)}, \ldots, \lambda_N^{(\omega)} > 0$, and explores temporal properties in the time series of $\{\lambda_i^{(\omega)}\}$ [11]. The window size ω has to be sufficiently small to guarantee a good resolution of the temporal variation of the $\lambda_i^{(\omega)}$'s, but sufficiently large in order to have a reliable estimation (see Refs. [19,24,25]). Further details about the choice of ω's value and its influence on the numerical results are given in Sec. IV A. The sharp transition towards $\lambda_i^{(\omega)} \approx 0$ observed earlier motivates the classification in regimes of motion [9,10]. For a system with N degrees of freedom, the trajectory is in a regime of type S_M if it has M local Lyapunov exponents $\lambda_i^{(\omega)} > \varepsilon_i$, where $\varepsilon_i \ll \lambda_i^{(\infty)}$ are small thresholds. Thereby, S_0 and S_N are *ordered* and *chaotic* regimes respectively. Regimes S_M with $0 < M < N$ are called *semiordered*. For the computation of the FTLLEs we use the traditional Benettin algorithm [33,34], which includes the Gram-Schmidt re-orthonormalization procedure. On average, the FTLLEs are in decreasing order. However, inversions of the order $\lambda_{i+1}^{(\omega)} > \lambda_i^{(\omega)}$ may happen for some times t and we have chosen to impose the order of $\lambda_i^{(\omega)}$ for all t.

A. Uncoupled case: $N = 1$

To get a better understanding of the involved complexity in the dynamics and the behavior of the FTLLEs, Fig. 1 displays the phase-space dynamics for a chaotic trajectory for one uncoupled ($\xi = 0$) SM together with the corresponding positive FTLLE $\lambda_1^{(\omega)}$ (see color bar) for $\omega = 100$. In this case the Lyapunov spectrum has only two Lyapunov exponents of which, asymptotically, one is positive and the other one negative. Thus, only two regimes are observed: (i) the ordered one, if $\lambda_1^{(\omega)} < \varepsilon_1$, and (ii) the chaotic one, if $\lambda_1^{(\omega)} > \varepsilon_1$. While the upper row in Fig. 1 presents the $K = 0.60$ case, the lower row shows results for $K = 0.65$. For both cases, the phase space has a large regular island located in the center, surrounded by higher-order resonances. In Fig. 1(a) we observe a 6-order resonance and in Fig. 1(e) an 8-order resonance [better seen in Figs. 1(b) and 1(f), respectively]. It is well known that additional higher-order resonances (not visible on the scale of these panels) live around the island. These islands lead to the dynamical trapping which can be stronger, or not, depending on the topological structure of the islands. Such dependency becomes more visible when the positive FTLLE $\lambda_1^{(\omega)}$ is calculated for the trajectories. This is shown in color in Figs. 1(b) and 1(f) with some magnifications (see black boxes) shown respectively in Figs. 1(c), 1(d) and 1(g), 1(h). We observe that, when approaching the island borders, the FTLLE decreases, as specified by the color bars in Figs. 1(d), 1(h). A very complex behavior is evident and only motions very close to the regular islands have smaller FTLLEs. This suggests that these motions close to the regular islands will belong to the ordered motion.

B. Coupled case: $N = 2$

A nice visualization of the regimes becomes clear when two coupled SMs are analyzed in phase space, as shown in Fig. 2. Different colors represent points $\boldsymbol{x}_t \in S_M$ belonging to regimes S_0 (blue circles), S_1 (red points), and S_2 (green points). These points were computed starting with a single

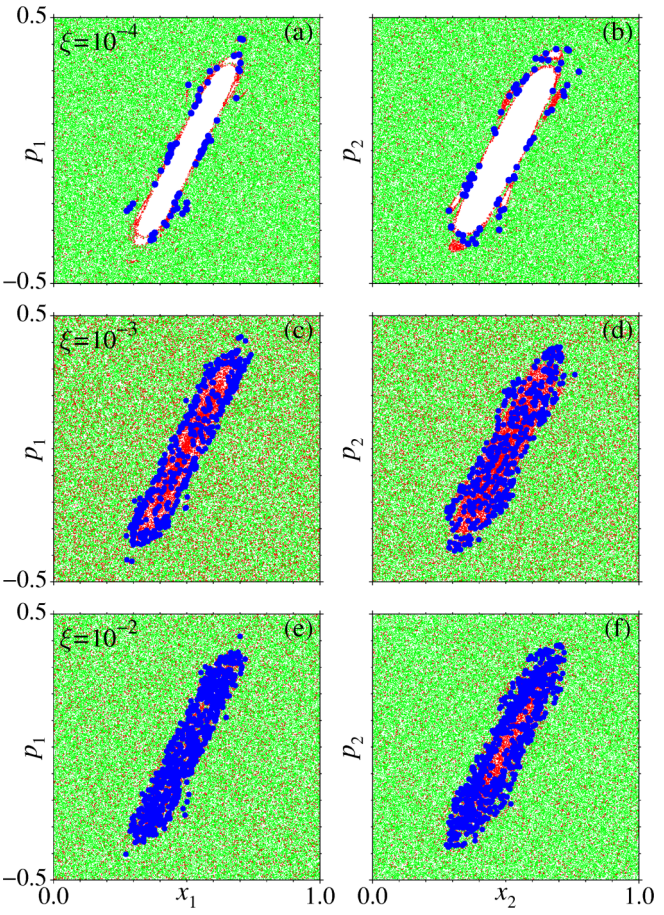

FIG. 2. Phase-space dynamics projected in (x_1, p_1) [(a), (c), and (e)] and in (x_2, p_2) [(b), (d), and (f)] for different values of ξ.

trajectory in the chaotic sea of the coupled system and iterating it 10^7 times. Table I presents the values of K_i used in the simulations and the thresholds ε_i used to define the regimes of motion. Blue circles are the points in phase space (x_1, p_1, x_2, p_2) for which $\lambda_i^{(\omega)} < \varepsilon_i$, for $i = 1, 2$. The red color indicates points for which $\lambda_1^{(\omega)} > \varepsilon_1$ and $\lambda_2^{(\omega)} < \varepsilon_2$. Green points are used if both FTLLEs are larger than the respective thresholds ε_i. We observe in Fig. 2 that by increasing the

TABLE I. Values of K_i used to couple the standard maps and the thresholds ε_i.

Value of K_i	$N = 2$	$N = 3$	$N = 4$	$N = 5$
K_1	0.65	0.65	0.65	0.65
K_2	0.60	0.63	0.64	0.64
K_3		0.60	0.63	0.63
K_4			0.62	0.62
K_5				0.61
Threshold	$N = 2$	$N = 3$	$N = 4$	$N = 5$
ε_1	0.10	0.10	0.10	0.10
ε_2	0.05	0.08	0.08	0.08
ε_3		0.05	0.06	0.07
ε_4			0.04	0.06
ε_5				0.04

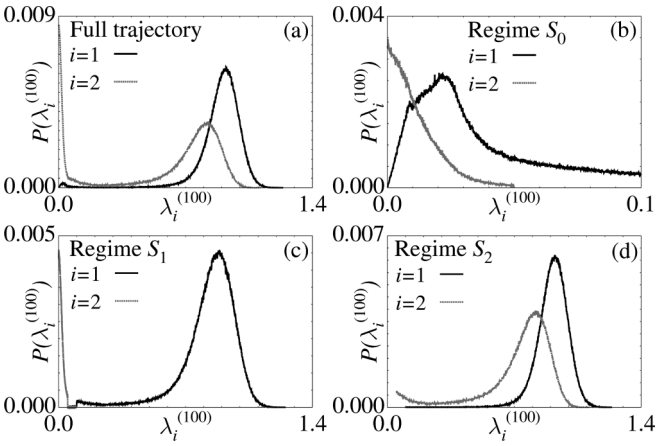

FIG. 3. Distributions $P(\lambda_i^{(\omega=100)})$ of the spectrum of FTLLEs $\{\lambda_i^{(\omega=100)}\}$ $(i = 1, 2)$ for the case $N = 2$ with $\xi = 10^{-3}$, obtained using 10^6 values of $\lambda_i^{(\omega=100)}$. The full trajectory was considered in (a). In (b), (c), and (d) only the regimes S_0, S_1, and S_2 were considered, respectively.

value of the coupling strength ξ, the trajectory penetrates the regular domain from the uncoupled case where there is the island's hierarchy, inside which only S_0 and S_1 regimes occur. Thus, by increasing the coupling force between the maps, the number of points which induce sticky motion increases.

In Fig. 3 we show the distributions $P(\lambda_i^{(\omega=100)})$ $(i = 1, 2)$ for the coupled case $N = 2$ with $\xi = 10^{-3}$. Considering a full trajectory initialized in the chaotic sea, the distributions of the FTLLEs $\lambda_i^{(\omega=100)}$ are bimodal [24,25], as we can see in Fig. 3(a). However, using our filtering procedure, it is possible to separate the different behaviors found in Fig. 3(a). For instance, in Fig. 3(b) only the regime S_0 was considered, and the profile of the resulting distribution of the FTLLE $\lambda_i^{(\omega=100)}$ is similar to the profile of the long tail ($\sim$0) of the $P(\lambda_i^{(\omega=100)})$ for the full trajectory. On the other hand, Fig. 3(d) shows the distributions for the chaotic regime S_2 and, in this case, we can see that values of $\lambda_i^{(\omega=100)} \sim 0$ are excluded. As result we obtain a Gaussian-like distribution, characteristic of cases where no sticky regions exist [24]. In Fig. 3(c) we plotted $P(\lambda_i^{(\omega=100)})$ for the semiordered regime S_1, the case for which $\lambda_1^{(\omega=100)} > \varepsilon_1$ and $\lambda_2^{(\omega=100)} < \varepsilon_2$.

C. Stickiness synchronization

From the above results it is easy to verify that for the ordered regime the positions of the coupled maps tend to be very close to the almost regular domains and to each other. This can be checked more precisely by determining, for $N = 2$ for example, the distance $|x_1 - x_2|$ as a function of time. This is shown by the gray dotted line in Fig. 4 for two distinct time windows. At a given time, the distance $|x_1 - x_2|$ suddenly approaches zero, leading to an approximated synchronization of the positions of the coupled SMs. Since these positions are not exactly equal, we say we have a synchronized-like state. In both cases the synchronization occurs only for a finite-time window. Surprisingly these time windows match those

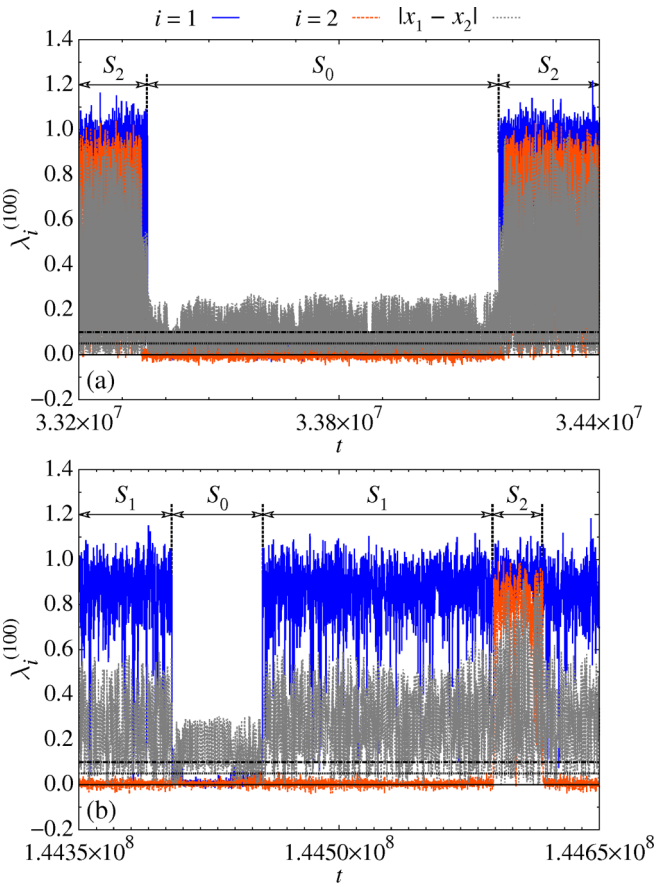

FIG. 4. Time series of the spectrum of FTLLEs $\{\lambda_i^{(\omega=100)}\}$ $(i = 1, 2)$ for the maps (1)–(2) with $N = 2$ and $\xi = 10^{-3}$. In (a) and (b) the thresholds $\varepsilon_1 = 0.1$ and $\varepsilon_2 = 0.05$ are represented by black dash-dotted and black dotted lines, respectively. The gray dotted line indicates the distance $|x_1 - x_2|$ and shows the synchronization of the maps $i = 1$ and $i = 2$ in the intervals of time for which the regime S_0 occurs.

times for which the ordered regime S_0 is present. This can be checked in the same picture, where we plot simultaneously the two positive FTLLEs $\lambda_i^{(\omega)}$ as a function of time. Thus, synchronization of the position of the maps coincides with the full synchronization of the FTLLEs. For the regime S_1 we observe in Fig. 4(b) that the distance $|x_1 - x_2|$ is more away from zero than this distance measured in the regime S_0, leading to a kind of "weaker" synchronization. In this case we say we have a *partial* synchronization, since only one FTLLE tends to zero. For S_2 there is no synchronization.

The relation between the position synchronization of the coupled maps shown above allows us to use the concept of *stickiness synchronization*. We have checked this relation for all S_0 regimes along a chaotic trajectory of length $t = 10^9$. Since all regimes S_M with $M < N$ are transient, and there is an intermittent transition between these regimes, we say we have ISS. Our results for higher dimensions can also be interpreted as the synchronization of FTLLEs. It is in fact a consequence of the synchronization of local expansion and contraction rates along all unstable and stable direction manifolds.

IV. QUALITATIVE DESCRIPTION OF ISS

Numerical techniques used to characterize the sticky motion can now be used to describe the qualitative behavior of the ISS decay in time. For this we use the consecutive time τ_M spent by a trajectory in the same regime S_M [11]. During a trajectory of length t_L we collected a series of τ_M and important results are obtained by analyzing the cumulative distribution of τ_M, defined as

$$P_{\rm cum}(\tau_M) \equiv \sum_{\tau'_M=\tau_M}^{\infty} P(\tau'_M). \tag{3}$$

Applying this alternative procedure to obtain the $P_{\rm cum}(\tau_M)$, we are able to estimate the decay exponent for the recurrence times. This technique is much more appropriate to estimate such an exponent when compared to the former one, based on the cumulative distribution of Poincaré recurrence times (or RTS), since it remains unclear how to estimate the timescale over which a higher-dimensional system reaches its asymptotic regime under the process of weak Arnold diffusion [5]. As this technique is based on a filtering process, we can select the events related to longer correlations and then obtain decay curves with several decades. In addition, there is no more dependence on the choice of recurrence set to obtain the RTS [35].

A. Uncoupled case: $N = 1$

To apply the filtering method we have to specify the threshold ε and the time window ω. Figures 5(a) and 5(b) compare the cumulative distribution $P_{\rm cum}(\tau_M)$ for the regime S_0, obtained using $\omega = 100$ and two values of ε, with the RTS $P_{\rm cum}(\tau)$, both quantities calculated for uncoupled SMs with two different values of K, specified in Fig. 5. For the determination of the RTS (gray solid curve) we have (i) used a recurrence region in the chaotic component of the phase space delimited by $0 < x < 1$ and $0.45 < p < -0.45$, and (ii) collected the lapses of time τ spent outside the recurrence region by a trajectory started inside such predefined box. Straight lines in Fig. 5 are consequences of the sticky motion. We realize that while the usual RTS presents some oscillations as a function of τ, leading to difficulties in the precise decay exponent, the filtering method *tends* to decrease such oscillations, mainly if the threshold $\varepsilon = 0.07$ is used. These results show that, for practical implementations, the thresholds can be defined as $\varepsilon_i \approx 0.10\langle\lambda_i^{(\omega)}\rangle$, where $\langle\ldots\rangle$ denotes the average over t, where $t = 1, \ldots, t_L$.

It is important to define how sensitive these results are in relation to the time window ω used to calculate the FTLLEs. For this, we compare $P_{\rm cum}(\tau_0)$ obtained using $\omega = 100$ and $\varepsilon = 0.07$ [blue dashed curves in Figs. 5(a) and 5(b)] with $P_{\rm cum}(\tau_0)$ for $\omega = 50$ and $\omega = 200$, keeping the threshold $\varepsilon = 0.07$. Figures 5(c) and 5(d) show this comparison for the cases $K = 0.60$ and $K = 0.65$, respectively, and the results demonstrate that even though the choice of ω may affect quantitatively the cumulative distributions $P_{\rm cum}(\tau_M)$, our conclusions about the algebraic decay obtained for the regime S_0 are not changed by oscillations around the chosen value $\omega = 100$ [11].

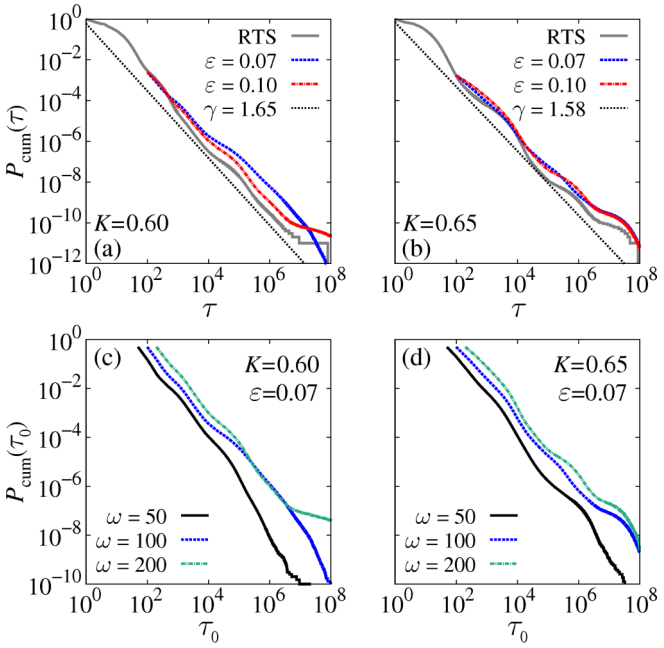

FIG. 5. Comparison between the filtering method and the RTS (gray solid curve) for the uncoupled case ($\xi = 0$) in (a) for $K = 0.60$ and in (b) for $K = 0.65$. The blue dashed and red dash-dotted curves are the cumulative distribution $P_{\rm cum}(\tau_0)$ of consecutive times τ_0 in the regime S_0 (normalized for convenience of scale), obtained for 10^{11} values of τ_M, using two different values of threshold ε. The RTS $P_{\rm cum}(\tau)$ was obtained for 10^{12} recurrences. In (c) and (d) we compare $P_{\rm cum}(\tau_0)$ for different values of ω.

B. Coupled cases: $N = 2, 3, 4, 5$

We start determining the cumulative distribution $P_{\rm cum}(\tau_M)$ for the $N = 2$ case for which we have regimes S_0, S_1, and S_2. This is shown in Fig. 6(a) for coupling $\xi = 10^{-3}$ and using values of K_i and ε_i according to Table I. It shows that the only power-law decay occurs for the S_0 regime. Thus, while full SS occurs for S_0 regimes with a power-law decay of the $P_{\rm cum}(\tau_M)$, all other regimes have a chaotic component leading to an exponential decay. This indicates that only full FTLLEs synchronized states tend to occur for consecutive very long times, even though with small probability.

Looking at the distributions $P_{\rm cum}(\tau_M)$ in Fig. 6(a), we observe for the semiordered regime $M = 1$ an exponential tail after an initial power-law decay with scaling $\beta \approx 0.5$ [15]. When the full SS takes place ($M = 0$), $P_{\rm cum}(\tau_0) \propto \tau_0^{-\gamma}$, with $\gamma = 1.16$. As shown in Fig. 6(b), this scaling is compatible with the result obtained using RTS. However, the cumulative distribution $P_{\rm cum}(\tau_0)$ provides a better characterization of algebraic decay (over several orders of magnitude), which is essential when dealing with high-dimensional systems (which may contain different pre-asymptotic regimes) and for an accurate estimation of the stickiness exponent γ. In Fig. 6(c) we show that $P_{\rm cum}(\tau_0)$ for the coupled case remains (qualitatively) the same for different values of ω around $\omega = 100$.

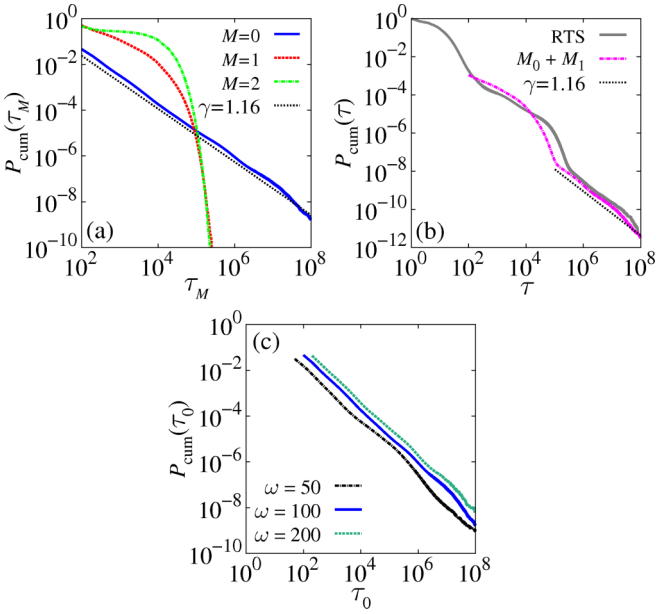

FIG. 6. (a) The cumulative distribution $P_{\rm cum}(\tau_M)$ of times τ_M for the regime S_M for the maps (1)–(2) with $N = 2$ and $\xi = 10^{-3}$, obtained using 2×10^{10} values of τ_M. The values of K_i and ε_i used are indicated in Table I. (b) Comparison between our method and the analysis based on RTS for the case $N = 2$ and $\xi = 10^{-3}$. The result obtained combining the curves $M_0 + M_1$ (normalized for convenience of scale) is equivalent to cumulative distribution $P_{\rm cum}(\tau)$, obtained for 10^{12} recurrences. In (c) we compare $P_{\rm cum}(\tau_0)$ for different values of ω.

Another very interesting quantity to be studied is the residence time $P(S_M)$ in each regime as a function of the coupling strength, defined by

$$P(S_M) = \frac{1}{\beta} \sum_{t=0}^{t_L} \delta_{t \in S_M}, \tag{4}$$

where $\beta = t_L/\omega$ is the factor of normalization. In Eq. (4), $\delta_{t \in S_M} = 1$ if in time t the trajectory is in the regime S_M, and $\delta_{t \in S_M} = 0$ otherwise. The $P(S_M)$ is shown in Fig. 7(a) for $N = 2$, in Fig. 7(b) for $N = 3$, in Fig. 7(c) for $N = 4$, and in Fig. 7(d) for $N = 5$. For smaller couplings ($\xi \lesssim 3 \times 10^{-2}$) the residence time decreases with M, namely $P(S_N) > P(S_{N-1}) > \ldots > P(S_M) > \ldots > P(S_1) > P(S_0)$. This means that the probability of finding the ordered regimes ($M = 0$) is much smaller when compared to semiordered regimes ($0 < M < N$) and so on. For larger couplings $\xi > 10^{-1}$, the probabilities of finding ordered and semiordered regimes have roughly the same values and tend to decrease until zero. Only the probabilities of fully chaotic regimes S_N remain for larger values ξ. It is important to mention that $P(S_M)$ corresponds to the (normalized) volume of the region related to regime S_M in the bounded phase space Γ. Hence the measure of the sticky region is given by $\mu(S_0) \sim \mu(\Gamma_{\rm tori}) \approx P(S_0)/[1 + P(S_0)]$, as explicitly demonstrated in Ref. [11] for small couplings $\xi \approx 0$.

From Figs. 6 and 7 we conclude that even though the probability of finding the full SS is small compared to the partial SS, it can occur for very long times due to the power-law decay found for $P_{\rm cum}(\tau_0)$. In addition we mention that, in distinction to usual synchronization found in dissipative systems, here the ISS tends to decrease for larger coupling between the maps [36].

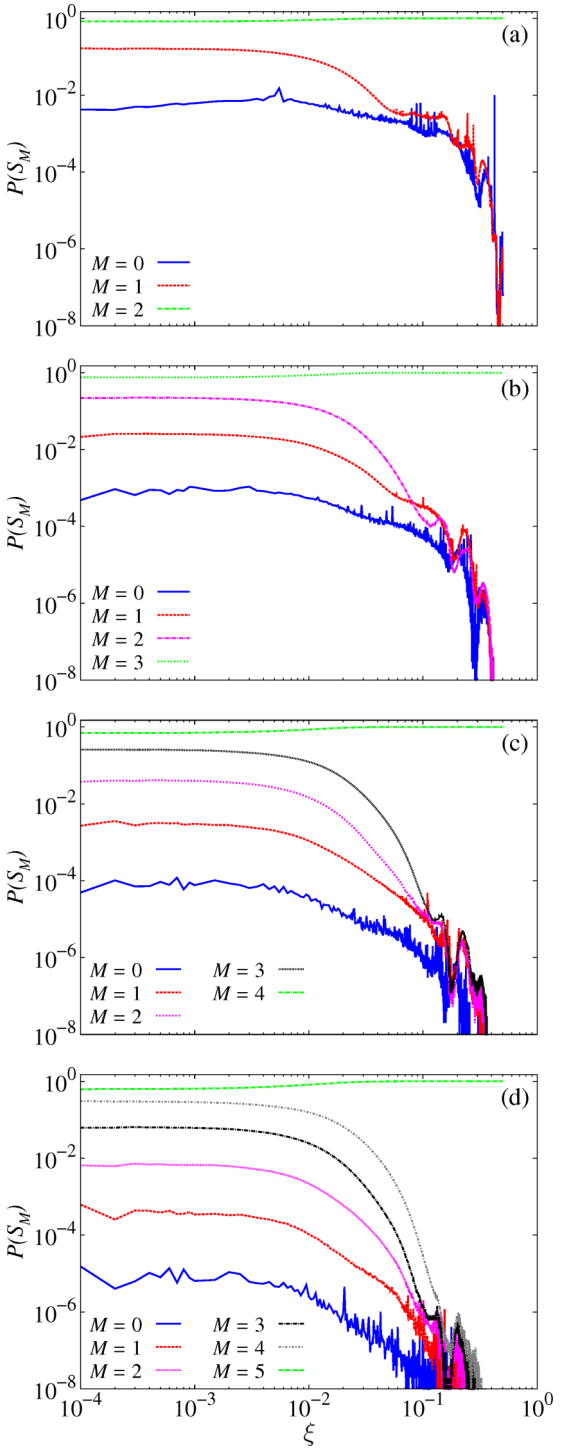

FIG. 7. Residence time in each regime S_M using $\omega = 100$ and (a) $N = 2$, (b) $N = 3$, (c) $N = 4$, and (d) $N = 5$. For each value of ξ, $P(S_M)$ was computed using a trajectory with length $t_L = 10^{10}$. The values of K_i and ε_i used in each case can be found in Table I.

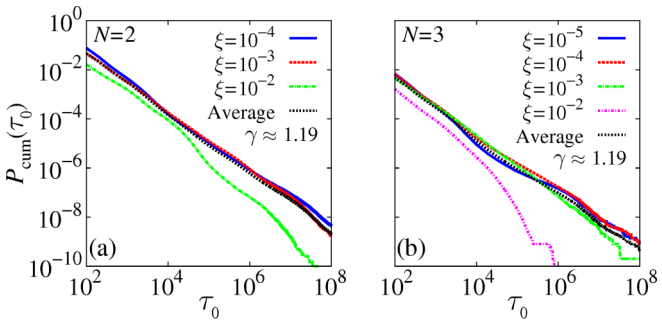

FIG. 8. The cumulative distribution $P_{\rm cum}(\tau_0)$ of consecutive times τ_0 in the regime S_0 using different values of coupling ξ for (a) $N = 2$ with 2×10^{10} values of τ_M and (b) $N = 3$ with 5×10^9 values of τ_M. The K_i and ε_i used in each case are indicated in Table I.

C. Characterizing the decay of synchronization: The ordered regime

The next step is to precisely quantify the ISS decay for distinct values of coupling ξ between $N = 2, 3, 4$, and 5 SMs. For this we used only the regime S_0, which is directly related with the full synchronization between the positions x_i. As demonstrated in Figs. 5(a), 5(b), and 6(b), the decay of $P_{\rm cum}(\tau_0)$ provides an amazing characterization of the sticky motion and allows obtaining accurately the exponent γ, so that the RTS analysis becomes needless. The results of this study are shown in Fig. 8(a) for $N = 2$ and in Fig. 8(b) for $N = 3$, using distinct values of ξ, as specified in the figure. The black dotted line is the average over all couplings of each case and fitting this curve we obtain a power-law decay with well-defined exponent $\gamma \approx 1.19$, observed for 6 decades. For $\xi = 10^{-2}$, long-term trappings tend to disappear. It is worth mentioning that the disappearance of the long-term sticky motion manifests itself in the increasing lack of data for S_0 as the coupling increases.

To finish we would like to present results for $N = 4$ and $N = 5$. Figure 9 displays the cumulative distribution $P_{\rm cum}(\tau_0)$ for the regime S_0 and for distinct coupling values, specified in the figure. We observe that for values of $\xi \leqslant 10^{-4}$ the exponent approaches $\gamma \approx 1.19$ for almost 6 decades in Fig. 9(a), and $\gamma \approx 1.22$ in Fig. 9(b), values obtained fitting the black dotted line that is the average over all couplings. The amount of long-term sticky motion decreases for $\xi > 10^{-4}$ in both cases. Again, this manifests itself in the increasing lack of data for S_0. However, since we still have at least three decades of power-law behavior, it can still be characterized as sticky motion leading to the full SS.

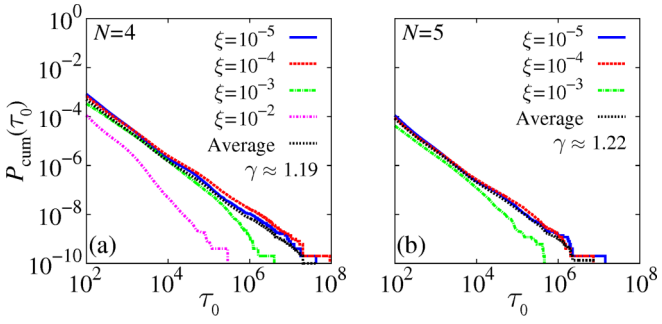

FIG. 9. The cumulative distribution $P_{\rm cum}(\tau_0)$ of consecutive times τ_0 in the regime S_0 using different values of coupling ξ for (a) $N = 4$ and (b) $N = 5$, both cases collecting 5×10^9 values of τ_M. The K_i and ε_i used in each case are indicated in Table I.

V. CONCLUSIONS

This work analyzes qualitatively the intermittent stickiness synchronization (ISS) decay in high-dimensional generic Hamiltonian systems. Such synchronization is generated by the regular structures on the chaotic trajectory, and can also be interpreted as the synchronization of FTLLEs. It is a synchronization of local expansion and contraction rates along all unstable and stable direction manifolds. We connect the intermittent motion between ordered, semiordered, and chaotic dynamical regimes with, respectively, the full, partial, and absence of synchronization generated by stickiness. By using the cumulative distribution of the consecutive times τ_M spent in each regime S_M, we demonstrate the ability of the recently proposed filtering procedure [11] to precisely characterize the ISS decay generated by the sticky motion. We also show that even though the residence time in the full SS state is small compared to the residence times in the partial SS states, it may occur for consecutive very long times due to the power-law decay of the $P_{\rm cum}(\tau_0)$.

In addition, our numerical results demonstrate that the algebraic decay exponent tends to $\gamma \approx 1.20$ for higher-dimensional systems. This is completely in agreement with the estimated decay exponent of time correlations $\chi \approx 0.20$ (both exponents are related by the well-known relationship $\chi = \gamma - 1$) obtained in [27] for $N = 2, 3$ symplectic maps interacting through a nearest-neighbor coupling scheme. The estimated decay exponents in these two works were obtained through three different approaches and are somewhat smaller than recent estimates [16] (such observations suggest a universality conjecture, at least for a moderate number of coupled Hamiltonian maps).

Future investigations can analyze a possible relation between the ISS observed here and the hydrodynamic modes found in many-body systems [37]. They present slow, long-wavelength behavior in the tangent-space dynamics. In addition, the properties of the covariant Lyapunov vectors [38–41] at the full SS might also be promising from the theoretical point of view and in applications.

ACKNOWLEDGMENTS

This study was financed in part by the Coordenação de Aperfeiçoamento de Pessoal de Nível Superior–Brasil (CAPES)–Finance Code 001. C.M. and M.W.B. thank CNPq (Brazil) for financial support. The authors also acknowledge computational support from Prof. C. M. de Carvalho at LFTC-DFis-UFPR (Brazil).

[1] A. Hampton and D. H. Zanette, Phys. Rev. Lett. **83**, 2179 (1999).
[2] U. E. Vincent, New J. Phys. **7**, 209 (2005).
[3] S. Boccaletti, J. Kurths, G. Osipov, D. Valladares, and C. Zhou, Phys. Rep. **366**, 1 (2002).
[4] L. M. Pecora and T. L. Carroll, Chaos **25**, 097611 (2015).
[5] A. J. Lichtenberg and M. A. Lieberman, *Regular and Chaotic Dynamics* (Springer-Verlag, New York, 1992).
[6] G. M. Zaslavsky, *Hamiltonian Chaos and Fractional Dynamics* (Oxford University Press, New York, 2008).
[7] B. V. Chirikov and D. L. Shepelyansky, Physica D **13**, 395 (1984).
[8] R. Artuso, Physica D **131**, 68 (1999).
[9] G. Contopoulos, L. Galgani, and A. Giorgilli, Phys. Rev. A **18**, 1183 (1978).
[10] A. Malagoli, G. Paladin, and A. Vulpiani, Phys. Rev. A **34**, 1550 (1986).
[11] R. M. da Silva, C. Manchein, M. W. Beims, and E. G. Altmann, Phys. Rev. E **91**, 062907 (2015).
[12] C. Manchein, M. W. Beims, and J. M. Rost, Chaos **22**, 033137 (2012).
[13] S. Mahata, S. Das, and N. Gupte, Phys. Rev. E **93**, 062212 (2016).
[14] G. Cristadoro and R. Ketzmerick, Phys. Rev. Lett. **100**, 184101 (2008).
[15] E. G. Altmann and H. Kantz, Europhys. Lett. **78**, 10008 (2007).
[16] D. L. Shepelyansky, Phys. Rev. E **82**, 055202(R) (2010).
[17] S. Lange, M. Richter, F. Onken, A. Bäcker, and R. Ketzmerick, Chaos **24**, 024409 (2014).
[18] S. Lange, A. Bäcker, and R. Ketzmerick, Eur. Phys. Lett. **116**, 30002 (2016).
[19] H. Kantz and P. Grassberger, Phys. Lett. A **123**, 437 (1987).
[20] M. Falcioni, U. Marini Betollo Marconi, and A. Vulpiani, Phys. Rev. A **44**, 2263 (1991).
[21] T. Konishi and K. Kaneko, J. Phys. A: Math. Gen. **25**, 6283 (1992).
[22] K. Kaneko and T. Konishi, Physica D **71**, 146 (1994).
[23] S. Tomsovic and A. Lakshminarayan, Phys. Rev. E **76**, 036207 (2007).
[24] J. D. Szezech, S. R. Lopes, and R. L. Viana, Phys. Lett. A **335**, 394 (2005).
[25] M. Harle and U. Feudel, Chaos, Solitons & Fractals **31**, 130 (2007).
[26] R. Artuso and C. Manchein, Phys. Rev. E **80**, 036210 (2009).
[27] T. M. Oliveira, R. Artuso, and C. Manchein, Physica A (to be published).
[28] T. Laffargue, K.-D. N. T. Lam, J. Kurchan, and J. Tailleur, J. Phys. A **46**, 254002 (2013).
[29] C. Manchein, M. W. Beims, and J. M. Rost, Physica A **400**, 186 (2014).
[30] R. M. da Silva, M. W. Beims, and C. Manchein, Phys. Rev. E **92**, 022921 (2015).
[31] M. Ding, T. Bountis, and E. Ott, Phys. Lett. A **151**, 395 (1990).
[32] E. G. Altmann, Ph.D. thesis, Max-Planck Institut für Physik Komplexer Systeme, 2007.
[33] G. Benettin, L. Galgani, A. Giorgilli, and J.-M. Strelcyn, Meccanica **15**, 9 (1980).
[34] A. Wolf, J. B. Swift, H. L. Swinney, and J. A. Vastano, Physica D **16**, 285 (1985).
[35] M. Sala, R. Artuso, and C. Manchein, Phys. Rev. E **94**, 052222 (2016).
[36] J. F. Heagy, L. M. Pecora, and T. L. Carroll, Phys. Rev. Lett. **74**, 4185 (1995).
[37] C. Dellago, H. A. Posch, and W. G. Hoover, Phys. Rev. E **53**, 1485 (1996).
[38] F. Ginelli, P. Poggi, A. Turchi, H. Chaté, R. Livi, and A. Politi, Phys. Rev. Lett. **99**, 130601 (2007).
[39] A. Norwood *et al.*, J. Phys. A **46**, 254021 (2013).
[40] M. W. Beims and J. A. C. Gallas, Sci. Rep. **6**, 37102 (2016).
[41] M. W. Beims and J. A. C. Gallas, Phys. Chem. Chem. Phys. **20**, 18539 (2018).